frontiers | Frontiers in Physics

BRIEF RESEARCH REPORT
published: 26 April 2022
doi: 10.3389/fphy.2022.857274

Study on Physical and Mechanical Characteristics of Shear Band in Jinpingzi Landslide Region II

Yongjin Wu[1,2], *Shuling Huang*[2]*, *Ke Liu*[3], *Qing Zhang*[1] *and Hongyue Pan*[3]

[1]Department of Engineering Mechanics, College of Mechanics and Materials, Hohai University, Nanjing, China, [2]Key Laboratory of Geotechnical Mechanics and Engineering of Ministry of Water Resources, Changjiang River Scientific Research Institute, Wuhan, China, [3]China Three Gorges Construction Engineering Corporation, Wuhan, China

The shear band is an important portion of a landslide. Investigating the shear band's physical characteristics is one of the most significant challenges for landslide stability analysis and control. A systematic study of shear band in Jinpingzi landslide region II was conducted in this paper. The microscopic composition, deformation, strength, and creep characteristics are investigated by various experiments. In addition, CT visualization technology is utilized to monitor and scan the failure process of the shear band in real-time, as well as carry out studies on failure mechanisms. Furthermore, a constitutive model of the shear band is established as an alternative to the conventional Duncan and Chang model, which does not have this model's limitations. The associated research will broaden understanding of such a medium's properties, but it will also be highly useful for stability analysis, deformation prediction, and prevention of such soil-rock mixture landslides.

Keywords: Jinpingzi landslide region II, shear band, soil-rock mixture, CT, physical characteristics, constitutive model

OPEN ACCESS

Edited by:
Qingxiang Meng,
Hohai University, China

Reviewed by:
Shaobo Chai,
Chang'an University, China
Yucong Pan,
Wuhan University, China

***Correspondence:**
Shuling Huang
huangsl@mail.crsri.cn

Specialty section:
This article was submitted to Interdisciplinary Physics, a section of the journal Frontiers in Physics

Received: *18 January 2022*
Accepted: *28 March 2022*
Published: *26 April 2022*

Citation:
Wu Y, Huang S, Liu K, Zhang Q and Pan H (2022) Study on Physical and Mechanical Characteristics of Shear Band in Jinpingzi Landslide Region II. Front. Phys. 10:857274. doi: 10.3389/fphy.2022.857274

INTRODUCTION

Landslides form and occur as a result of a dynamic mechanical process that includes the accumulation of slope deformation, local damage, and the expansion, penetration, and sliding of the failure surface [1–3]. The shear band is an important portion of a landslide that is highly related to the deformation and stability of the landslide [4]. One of the main challenges to be tackled in landslide stability analysis and control is the investigation of its physical and mechanical properties. The sliding mass of accumulation landslides is soil-rock mixtures formed by Quaternary or recent loose accumulations [5], and they have specific development patterns, deformation, and damage characteristics. The soil-rock mixture is highly inhomogeneous and discontinuous, with significant nonlinear features, as it is composed of various types of soil and gravel with varied grain sizes [6]. Furthermore, influence factors such as reservoir rise and fall, rainfall, and groundwater level changes will inevitably complicate its deformation and failure mechanism.

Many academics have conducted numerous studies to investigate the physical and mechanical properties of soil-rock mixtures, including large-scale *in situ* push shear tests, indoor direct shear tests, triaxial shear tests, and permeability coefficient tests [7–10]. The microstructure model of soil-rock mixture was established by mesoscopic image manipulation, and automatic finite-difference mesh generating technology [11–13]. The fractal law of particle size distribution of a soil-rock mixture was studied using fractal theory [14–16]. Changes in the microstructure of soil-rock mixtures are investigated with the application of CT visualization techniques [17, 18]. In general, the development of geotechnical constitutive modeling is to adopt the corresponding yield conditions

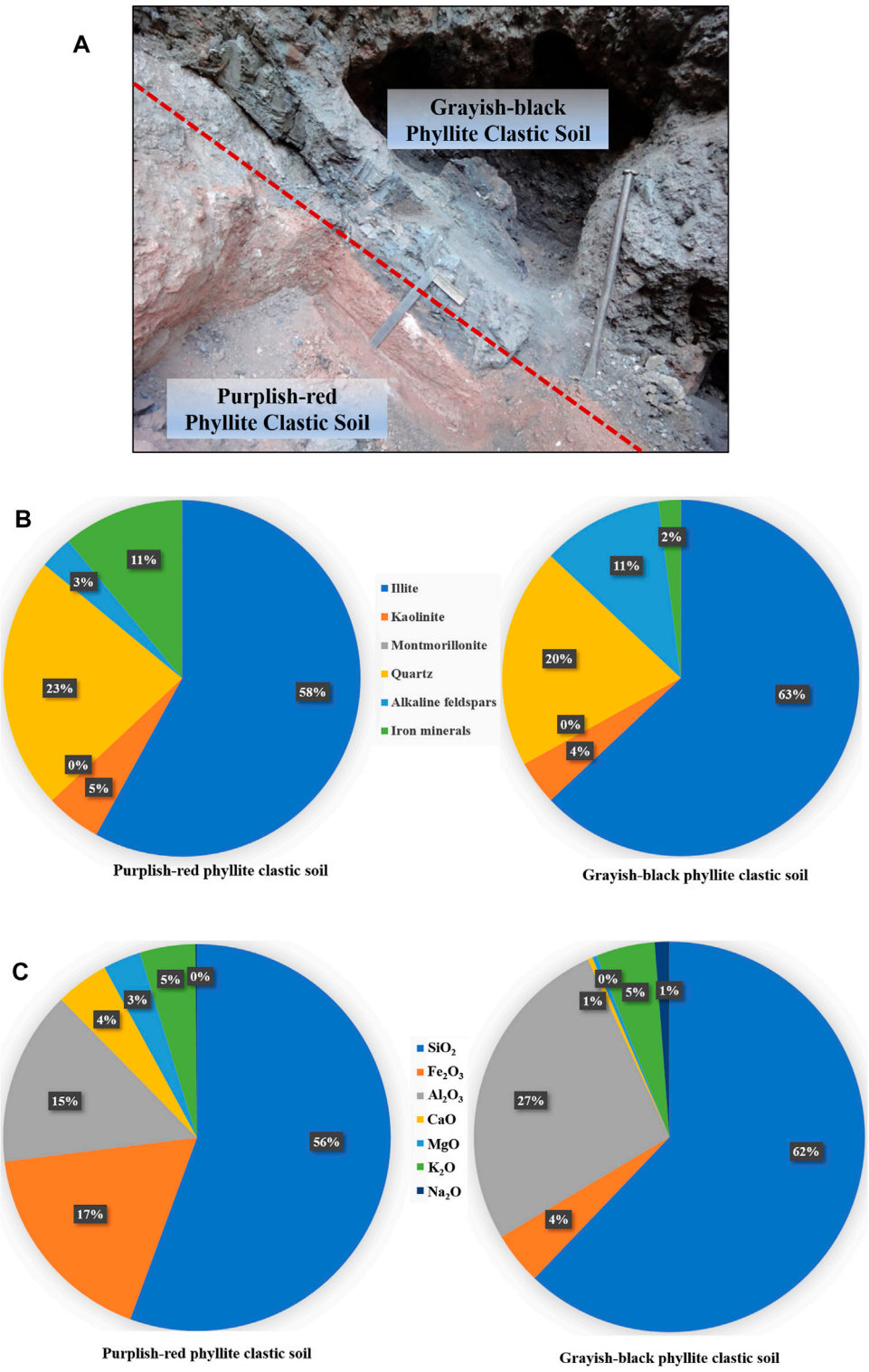

FIGURE 1 | Phyllite clastic shear band: **(A)** photograph; **(B)** mineral composition; **(C)** chemical composition.

according to the different types of geotechnical soils and to propose some mathematical models based on test results and extend them to the general cases, to establish a series of constitutive models that meet engineering reality [19–21]. Besides, the NMM was used to analyze the stability of the soil-rock-mixture slopes [22, 23].

Located on the right bank of the Jinsha River, Jinpingzi landslide region II is approximately 2,500 m away from the downstream of the Wudongde hydropower plant dam site. Region II is a large and creeping landslide, with a total area of around 0.6 km^2, a total volume of around $2,700 \times 10^4$ m^3, and an enormous height difference between the front and back edges, exceeding 650 m. Until at present, region II is significantly deformed, with weak stability and an overall creeping slip state. If large-scale instability occurs, the water level downstream may rise, threatening the normal operation of the power-producing system. The research shows that the deformation in region II is creeping slip along with the base-rock surface or phyllite clastic soil layer. The creeping slip mechanism of the shear band is exceedingly complicated and plays a controlling role in landslide sliding. To further establish a constitutive model and determine parameters of the soil-rock mixture in the shear band, as well as to accurately evaluate the effectiveness of control measures, it is necessary to investigate the physical and mechanical properties of the shear band. The microscopic composition, deformation, strength, and creep characteristics are investigated by various experiments. In addition, CT visualization technology is utilized to monitor and scan the failure process. Furthermore, a constitutive model of the soil-rock mixture is established as an alternative to the conventional Duncan and Chang model.

PHYSICAL AND MECHANICAL CHARACTERISTICS

The accumulation of Jinpingzi landslide region II can be separated into four layers from top to bottom. The first layer is a layer of dolomite block gravel with a tiny proportion of silt, and a thickness of 20–61 m. The second layer is a layer of phyllite debris with soil, and a thickness of 16–45 m. The third layer is a layer of phyllite debris soil that serves as a shear band, with a thickness of 2–9 m. The fourth layer is a layer of paleogully debris and gravel with a small amount of silt, with a thickness of 30–64 m.

The phyllite debris soil of the shear band is purple-red and gray-black silty clay with gravels. The soil is in a hard-plastic state, with a tight structure. The shear band's extrusion dislocation characteristics are very obvious, and the polished surface and scratches can be seen.

Microstructure

The hanging wall of the shear band is grayish-black phyllite clastic soil, and the footwall is the purplish-red one (**Figure 1A**). According to the mineral analysis results of soil-rock mixture samples in the shear band (**Figure 1B**), the mineral components in the purplish-red and grayish-black samples are primarily clay minerals, accounting for 60–70% of the total content (illite 55–65%), and other mineral components account for 30–45% (quartz 20–25%). According to the results of the mineral chemical analysis (**Figure 1C**), the Fe_2O_3 content of the purplish-red phyllite clastic soil is as high as 15.97%, which is significantly higher than that of the grayish-black one, while the organic matter content of the grayish-black clastic soil is higher, which is the major contributor to the difference in appearance color between the two. There is no discernible variation in the content of other minerals between them.

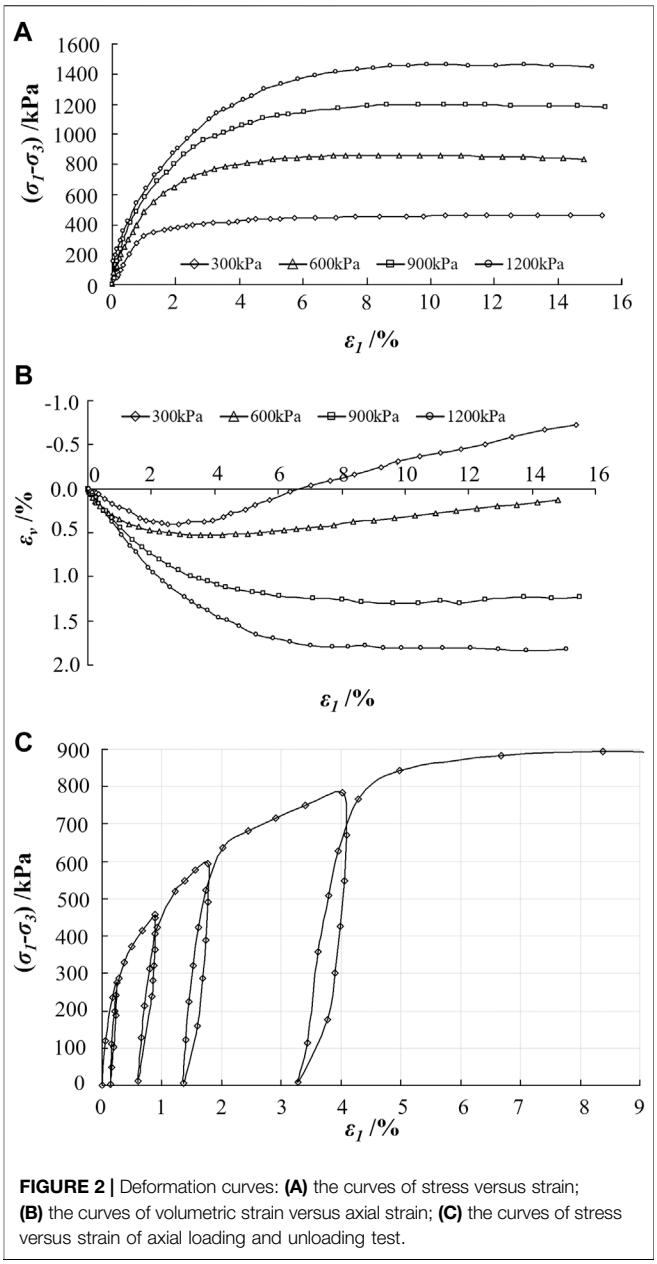

FIGURE 2 | Deformation curves: **(A)** the curves of stress versus strain; **(B)** the curves of volumetric strain versus axial strain; **(C)** the curves of stress versus strain of axial loading and unloading test.

The purplish-red phyllite clastic soil samples of the Shear band have a natural moisture content of 9.2–12.0% and a dry density of 2.09–2.19 g/cm^3. The grayish-black phyllite clastic soil samples have a natural moisture content of 11.8–13.3% and a dry density of 1.99–2.07 g/cm^3. The free expansion rate of fine material composition is 28–29%, indicating that they are all non-expansive soil. The permeability coefficient of the undisturbed samples is small, which is 10e−6 cm/s orders of magnitude, playing a role in water insulation.

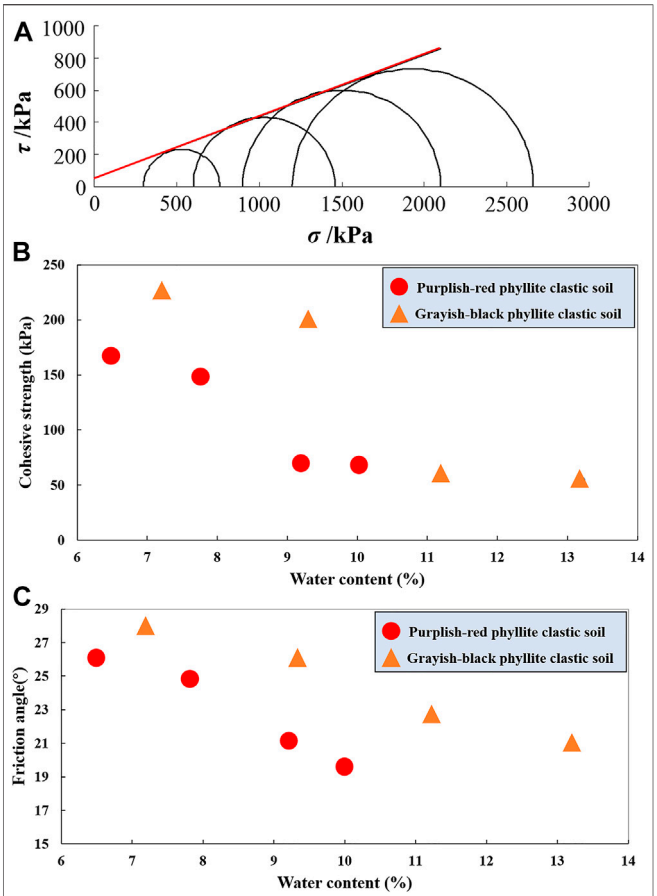

FIGURE 3 | Strength curves: **(A)** strength envelope; **(B)** relationship between cohesion and water content; **(C)** relationship between friction angle and water content.

Deformation Behavior

The stress-strain curves of phyllite clastic soil present obvious nonlinearity, indicating it is generally a hardening type (**Figure 2A**). The hardening phenomenon is more significant as the confining pressure increases.

Under low confining pressure, the volumetric-axial strain curves of phyllite clastic soil reveal a process of shear shrinkage followed by dilatancy (**Figure 2B**). With the increase of confining pressure and the decrease of water content, the volumetric strain-axial strain curves gradually show shear shrinkage. According to the preceding, the lower confining pressure and the higher water content the condition is, the more significant the dilatancy deformation in the triaxial test will be, or the volumetric deformation will transform from shear contraction to dilatancy.

In the axial loading and unloading tests, the elastic modulus decreases gradually as the stress level and loading and unloading periods increase, indicating that under these conditions, the increase in stress level and loading and unloading period causes damage accumulation in soil samples (**Figure 2C**).

In the isotropic loading and unloading tests, the volume rebound index and expansion index will gradually decrease with the increase of unloading confining pressure and loading and unloading periods. In other words, when all pressures are equal in all directions, increasing the unloading confining pressure and loading and unloading periods increases the unloading modulus, because, with the increased confining pressure and loading and unloading times, the soil would consolidate and densify.

Strength Property

Figure 3A shows the strength envelope of the sample, **Figure 3B** shows the relationship between cohesion and water content, and **Figure 3C** shows the relationship between friction angle and water content. The moisture content of purplish-red phyllite clastic soil samples of the Shear band increases from 6.5 to 10.0% (saturated state), cohesiveness decreases from 165.4 to 66.7 kPa, and the internal friction angle decreases from 26.2° to 19.7°. The moisture content of grayish-black phyllite clastic soil samples of the Shear band increases from 7.2 to 13.2% (saturated state), cohesiveness decreases from 225.8 to 54.4 kPa, and the internal friction angle decreases from 27.9° to 21.0°.

The cohesiveness and internal friction angle of the phyllite clastic soil of the Shear band decrease as the moisture content of the soil increases. The cohesiveness and starting moisture content curve, on the other hand, reveals a step-like steep decrease connection. When the moisture content is low, the cohesion-moisture content curve is relatively gentle, decreasing slightly with increasing moisture content; when the moisture content reaches a certain level, the cohesion drops sharply; when the moisture content approaches a saturated state, the cohesion remains essentially unchanged. With increasing moisture content, the internal friction angle reduces linearly.

Creep Property

When the shear load is low, the shear band samples exhibit decaying creep, and the shear displacement is primarily immediate, tending to be stable within 12 h. It is non-decaying creep when the shear stress is near to its fast shear strength value, and the creep curve is separated into three stages: immediate creep, constant-speed creep, and accelerated creep until the sample abruptly shears. The shear load has a large impact on this failure mechanism, and the duration is usually within 1–12 h.

From the beginning to the end, the creep of sliding soil samples can be divided into the following three stages. The first stage is instantaneous deformation during initial loading; that is, when shear stress is applied, the soils are instantaneously deformed, and the creep deformation rate rapidly decreases and approaches zero. The steady creep stage is the second stage, in which the shear displacement is almost constant and the creep deformation rate is nearly zero. The third stage is the direct failure stage or the accelerated failure stage, which primarily demonstrates that when the shear load reaches a certain level, the shear displacement suddenly increases, and the shear specimen experiences instantaneous shear slip failure, or at the final level of shear stress, the shear rate gradually increases, and the specimen experiences accelerated shear failure.

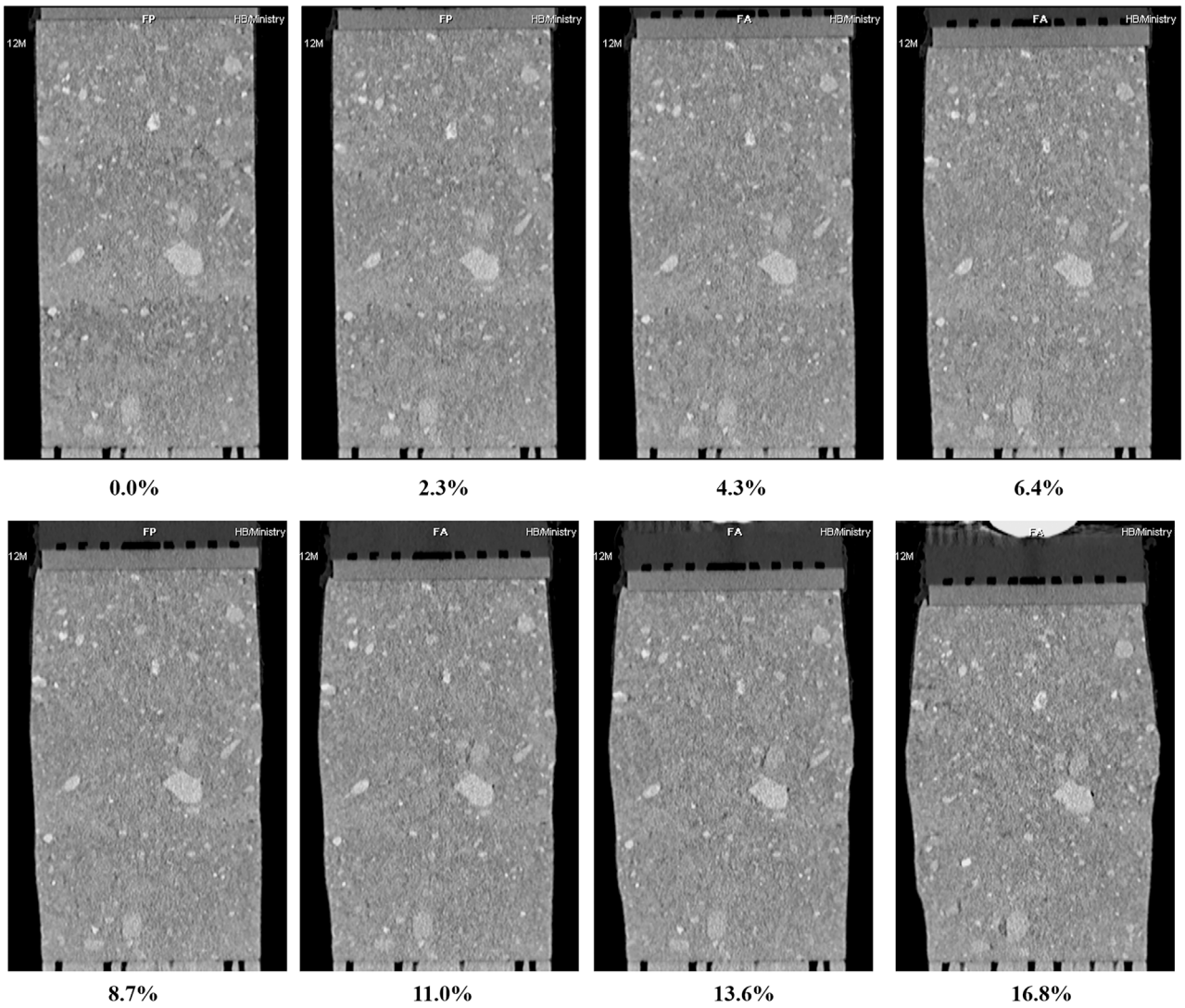

FIGURE 4 | CT triaxial test results.

CT VISUALIZATION OF MICROSCOPIC FAILURE PROCESS

CT triaxial testing is performed on a sample of phyllite clayey soil sliding belt, with the size of Φ101 mm × 200 mm, and the dry density of 2.05 g/cm^3. The confining pressures for the consolidation drainage exhaust shear test are 0.2, 0.3, and 0.6 MPa. Under the guidance of the strain loading method, the sample is scanned using CT when loading to a predefined strain until the strain reaches 15–20%. The CT images of samples of phyllite clastic soil under varied axial strains when confining pressure is 0.3 MPa and water content is 8.0% are shown in **Figure 4**.

The sample loading process is a progressive adjustment of particle position, with little change in geometric shape and size of particles and no evident particle breakup. The lateral displacement of particles is greatest in the center of the sample and gradually diminishes towards both ends. As the axial strain increases, the centre portion of the sample bulges outward, in the shape of a round drum.

Due to the pores in the sample, the initial stage of loading results in primary axial deformation of the particles. The sample bulges slightly as the axial strain increases and a local primary inclined crack of 60° forms in the center and upper section. As the axial strain continues to increase, the lateral bulge becomes more visible, with the appearance of another main crack, and the two primary cracks cross each other. Furthermore, when the two intersecting primary cracks become larger, many minor microcracks will form around them. When the axial strain reaches a certain value, an X-shaped or Y-shaped shear band could be seen in the sample, and the shear plane runs through the entire sample at 60° to the horizontal plane. At this time, plastic shear damage occurs in the sample.

The lower the moisture content and the lower the confining pressure, the more visible the outward bulging deformation of the sample and the X-type shear damage zone. The damage process of the sample is a process in which local cracks eventually penetrate to generate a whole slip surface. Due to the composition and non-uniformity of phyllite clastic soil, there are sometimes many secondary cracks piercing through during the penetration process.

The average and standard deviation of CT numbers are used to quantify the sample damage process. The CT's number average value is a reflection of density, which is the average value of the selected area in the image; the CT number's standard deviation is a reflection of density uniformity. The sample is compacted first under low strain, and as the strain increases, microcracks appear in the sample, which shows that the average value of CT numbers first slightly increases and then gradually decreases, whereas the standard deviation of CT numbers first slightly decreases and then gradually increases. Finally, the average value and standard deviation of CT numbers tend to be stable when there is an obvious shear band in the sample. The strain of microcracks in the CT statistics and the strain of macroscopically observed microcracks are not equal, so the CT number statistics is recommended to be the prevailing value in determining the strain of microcracks in the shear band.

MACROSCOPIC MECHANICAL CONSTITUTIVE MODEL

Based on the above-mentioned test results of the soil-rock mixture in the shear band, a constitutive model is established as an alternative to the conventional Duncan and Chang model [24, 25], which does not have this model's limitations. The model provides some features, including *1*) a Mohr-Coulomb failure criterion and flow rule, *2*) a friction hardening law, *3*) a dilation law based on Rowe stress dilatancy theory [26]. The constitutive model can demonstrate a realistic stress-strain connection at failure and post-failure.

Incremental Elastic Law

The elastic behavior of the constitutive model is expressed using generalized Hooke's law. The incremental function in terms of principal stress and strain is expressed as

$$\begin{cases} d\sigma_1 = \alpha \cdot d\varepsilon_1^e + \beta\left(d\varepsilon_2^e + d\varepsilon_3^e\right) \\ d\sigma_2 = \alpha \cdot d\varepsilon_2^e + \beta\left(d\varepsilon_1^e + d\varepsilon_3^e\right) \\ d\sigma_3 = \alpha \cdot d\varepsilon_3^e + \beta\left(d\varepsilon_1^e + d\varepsilon_2^e\right) \end{cases} \tag{1}$$

Where $\alpha = 3K_t(3K_t + E_t)/(9K_t - E_t)$, $\beta = 3K_t(3K_t - E_t)/(9K_t - E_t)$, and E_t and K_t are the tangent elastic modulus and tangent elastic bulk modulus, respectively. The variation of E_t and K_t are represented by the Duncan-Chang theory

$$E_t = K_a p_{ref}\left(\frac{\sigma_3}{p_{ref}}\right)^n \left[1 - \frac{R_f(\sigma_1 - \sigma_3)(1 - \sin\varphi)}{2c \cdot \cos\varphi + 2\sigma_3 \sin\varphi}\right]^2 \tag{2}$$

$$K_t = K_b P_{ref}\left(\frac{\sigma_3}{p_{ref}}\right)^m \tag{3}$$

Where parameters K_a and K_b are the experiment constant, and m and n are the constant modulus exponent $(m, n \le 1)$, and c is the cohesion, and φ is the friction angle, and P_{ref} is the reference pressure, and R_f is the failure ratio.

Composite Yield Criterion

Shear yielding is defined by the Mohr-Coulomb failure criterion with

$$f^s = \sigma_1 - \frac{1 + \sin\varphi_m}{1 - \sin\varphi_m}\sigma_3 + 2c \cdot \sqrt{\frac{1 + \sin\varphi_m}{1 - \sin\varphi_m}} \tag{4}$$

Where φ_m is the mobilized friction angle.

The potential function is nonassociated and has the form

$$g^s = \sigma_1 - \frac{1 + \sin\psi_m}{1 - \sin\psi_m}\sigma_3 \tag{5}$$

Where ψ_m is the mobilized dilation angle. A law based on Rowe dilatancy theory [11] is used to characterize ψ_m. The equation has the form

$$\sin\psi_m = \frac{\sin\varphi_m - \sin\varphi_{cv}}{1 - \sin\varphi_m \sin\varphi_{cv}} \tag{6}$$

$$\sin\varphi_{cv} = \frac{\sin\varphi_f - \sin\psi_f}{1 - \sin\varphi_f \sin\psi_f} \tag{7}$$

Where φ_f and ψ_f are ultimate friction angle and dilation angle, respectively.

The tensile yield function is expressed as

$$f^t = \sigma^t - \sigma_3 \tag{8}$$

Where σ^t is the tensile strength.

The potential function g^t corresponds to an associated flow rule, and has the form

$$g^t = -\sigma_3 \tag{9}$$

Hardening Law

Friction Hardening

The hyperbolic behavior between deviatoric stress versus axial strain obtained in a drained triaxial test is described by introducing a friction strain-hardening law. The plastic shear strain measure, γ^p, is defined by

$$d\gamma^p = \sqrt{\frac{\left(d\varepsilon_1^{dp}\right)^2 + \left(d\varepsilon_2^{dp}\right)^2 + \left(d\varepsilon_3^{dp}\right)^2}{2}} \tag{10}$$

Where $d\varepsilon_1^{dp}$, $d\varepsilon_2^{dp}$, and $d\varepsilon_3^{dp}$ are the principal, deviatoric, plastic shear-strain increments. The mobilized friction angle, φ_m is calculated in terms of the plastic shear strain measure, γ^p, by means of the following function

$$\varphi_m = \arcsin\left[\frac{\sin\varphi_f}{R_f}\left(1 - \frac{1}{1 + \gamma^p \frac{G_t}{p_m}\frac{R_f}{\sin\varphi_f}}\right)\right] \tag{11}$$

Where p_m is the mean stress, and G_t is the tangent elastic shear modulus, they are represented by the following equations

$$p_m = \frac{\sigma_1 + \sigma_2 + \sigma_3}{3} \tag{12}$$

$$G_t = \frac{3K_t E_t}{9K_t - E_t} \tag{13}$$

Shear Hardening

A dilation strain-hardening law is introduced to model the shear-induced compaction and dilation behavior. The shear-hardening flow function is expressed as

$$d\varepsilon_v^p = d\gamma^p \cdot \sin\psi_m \tag{14}$$

Where $d\varepsilon_v^p$ is the plastic volumetric strain increment. The mobilized dilation angle, ψ_m , is characterized by an equation based on Rowe stress-dilatancy theory.

CONCLUSION

The stress versus strain curves of phyllite clastic soil show obvious nonlinearity, indicating that it is generally strain-hardening type. The volumetric strain versus axial strain curves show compaction at first and then dilation under low confining pressure. As confining pressure and water content increase, the curves exhibit gradual contract. According to the above, the higher the water content and lower the confining pressure, the more obvious the dilatancy deformation of phyllite clayey soil in triaxial test.

The high presence of clay minerals in phyllite clastic soil, as well as the water-soaked softening, are the reasons of the decrease in cohesion and friction. The curves of cohesiveness versus initial water content exhibit a stepwise sharp decrease relationship. The curves are gentle in the low water content condition, and when the specified water content is reached, cohesion plunges. When the water content rises to a particular point, the cohesiveness remains constant. The friction angle decreases linearly as the water content increases.

During the creep of the phyllite clastic soil layer, the loose and permeable soil in the lower part gradually turned into a hard plastic over-consolidation state with dense structure *via* processes of grinding, compaction, and consolidation. The shear strength of the shear band's soil was improved and exhibited water-proof characteristics. In a general sense, the deformation of the sliding mass in region II is a dynamic adjustment and evolution process in which the physical properties of the phyllite clastic soil are correspondingly changed due to the change of mesostructured, rather than creeping.

DATA AVAILABILITY STATEMENT

The original contributions presented in the study are included in the article/Supplementary Material, further inquiries can be directed to the corresponding author.

AUTHOR CONTRIBUTIONS

YW and SH were in involved in the final development of the project. YW wrote the manuscript draft. KL analyzed the test data. HP provided relevant documents of Jinpingzi landslide. QZ provided the technical guidance. All authors: corrections, modifications, and final acceptance.

FUNDING

The authors declare that this study received funding from China Three Gorges Construction Engineering Corporation. The funder had the following involvement in the study: KL and HP are employed by China Three Gorges Construction Engineering Corporation. HP provided relevant documents of the Jinpingzi landslide. KL analyzed the test data. They were also involved in corrections, modifications, and final acceptance.

REFERENCES

1. Huang RQ. Large-scale Landslides and Their Sliding Mechanisms in China since the 20th century. *Chin J Rock Mech Eng* (2007) 3:433–54. doi:10.3321/j.issn:1000-6915.2007.03.001
2. Erismann TH. Mechanisms of Large Landslides. *Rock Mech* (1979) 12:15–46. doi:10.1007/BF01241087
3. De Blasio FV. *Introduction to the Physics of Landslides: Lecture Notes on the Dynamics of Mass wasting[M]*. Berlin, Germany: Springer Science & Business Media (2011).
4. Qiao JP. Structure and Shape of Landslide. *Chin J Rock Mech Eng* (2002) 9:1355–8. doi:10.3321/j.issn:1000-6915.2002.09.015
5. Liu C, Su LJ, Liu WJ. Review of Meso-Structure Characteristic of Soil-Rock Mixture in Accumulation Landslides. *Mt Res* (2015) 33(03):348–55. doi:10.16089/j.cnki.1008-2786.000044
6. Wang DJ, Tang HM, Li CD, Ge YF, Yi XL. Stability Analysis of Colluvial Landslide Due to Heavy Rainfall. *Rock Soil Mech* (2016) 37(02):439–45. doi:10.16285/j.rsm.2016.02.017
7. Zhou Z, Fu HL, Liu BS, Tan HH, Long WX. Orthogonal Tests on Permeability of Soil-Rock-Mixture Chinese. *J Geotech Eng* (2006) 09:1134–8. doi:10.3321/j.issn:1000-4548.2006.09.016
8. Huang B, Fu XD, Tan F, Wu ZM. Experimental Study of Relationship between Water Content and Strength or Deformation of Slip Soil. *Rock Soil Mech* (2012) 33(9):2613–8. doi:10.16285/j.rsm.2012.09.008
9. Jiang JS, Chen ZL, Lu WP, Zuo YZ, Ding HS. Strength Behavior of Coarse-Grained Soils Based on Large-Scale Triaxial Drained Shear Test. *Water Resour Power* (2014) 32(7):109–12.
10. You XH, Tang JS. Research on Horizontal Push-Shear Iin-Ssitu Test of Soil and Rock-Mixture. *Chin J Rock Mech Eng* (2002) 10:1537–40. doi:10.3321/j.issn:1000-6915.2002.10.021
11. Xu WJ, Wang YJ, Chen ZY, Hu RL. Stability Analysis of Soil-Rock Mixed Slope Based on Digital Image Technology. *Rock Soil Mech* (2008) S01:341–6. doi:10.3969/j.issn.1000-7598.2008.z1.069
12. Li X, Liao QL, He JM. In Situ tests and a Stochastic Structural Model of Rock and Soil Aggregate in the Three Gorges Reservoir Area, China. *Int J Rock Mech Mining Sci* (2004) 41(3):494–9. doi:10.1016/j.ijrmms.2003.12.030

13. You XH, He G, Li X. Meso-handling Technology of Earth-Rock Aggregate Slope. *Hydrogeol Eng Geol* (2003) 30(1):18–21. doi:10.3969/j.issn.1000-3665.2003.01.005
14. Xie HP. Fractal Pores and Fractal Particles of Rock and Soil Materials[J]. *Adv Mech* (1993) 23(2):145–64. doi:10.6052/1000-0992-1993-2-J1993-015
15. Wang Y, Li X. Study on Mesoscopic Fractal Feature and Mechanical Properties for Rock and Soil Aggregates Samples. *Chin J Rock Mech Eng* (2015) 34(S1):3397–407. doi:10.13722/j.cnki.jrme.2013.1527
16. Xu WJ, Hu RL. Particle Size Fractal Characteristics of the Soil-Rock Mixtures in the Right Bank Slope of Jinsha River at Long-Pan, Tiger-Leaping Gorge Area. *J Eng Geol* (2006) 14(4):496–501. doi:10.3969/j.issn.1004-9665.2006.04.011
17. Taina IA, Heck RJ, Elliot TR. Application of X-ray Computed Tomography to Soil Science: A Literature Review. *Can J Soil Sci* (2008) 88(1):1–19. doi:10.4141/CJSS06027
18. Zuo YZ, Chen ZL, Zhao N. Expansion Mechanism of Shear Bands in Phyllite Detritus Soil by CT Technology. *Chin J Geotechnical Eng* (2015) 37(8):1524–31. doi:10.11779/CJGE201508024
19. Zheng YR, Kong L. *Geotechnical Plastic Mechanics*. Beijing: China Building Industry Press (2010). p. 430.
20. Desai CS. Constitutive Modeling of Materials and Contacts Using the Disturbed State Concept: Part 1 - Background and Analysis. *Comput Structures* (2015) 146:214–33. doi:10.1016/j.compstruc.2014.07.018
21. Desai CS. Constitutive Modeling of Materials and Contacts Using the Disturbed State Concept: Part 2 - Validations at Specimen and Boundary Value Problem Levels. *Comput Structures* (2015) 146:234–51. doi:10.1016/j.compstruc.2014.07.026
22. Yang Y, Sun G, Zheng H, Yan C. An Improved Numerical Manifold Method with Multiple Layers of Mathematical Cover Systems for the Stability Analysis of Soil-Rock-Mixture Slopes. *Eng Geology* (2020) 264:105373. doi:10.1016/j.enggeo.2019.105373
23. Yang Y, Sun G, Zheng H, Qi Y. Investigation of the Sequential Excavation of a Soil-Rock-Mixture Slope Using the Numerical Manifold Method. *Eng Geology* (2019) 256:93–109. doi:10.1016/j.enggeo.2019.05.005
24. Duncan JM, Chang C-Y. Nonlinear Analysis of Stress and Strain in Soils. *J Soil Mech Found Div* (1970) 96(5):1629–53. doi:10.1061/JSFEAQ.0001458
25. Duncan JM. Factors of Safety and Reliability in Geotechnical Engineering. *J Geotech Geoenviron Eng* (2000) 126(4):307–16. doi:10.1061/(asce)1090-0241(2000)126:4(307)
26. Rowe PW. The Stress-Dilatancy Relation for Static Equilibrium of an Assembly of Particles in Contact. *Proc R Soc Lond A* (1962) 269(1339):500–27. doi:10.1098/rspa.1962.0193

Conflict of Interest: KL and HP were employed by China Three Gorges Corporation Limited, China.

The remaining authors declare that the research was conducted in the absence of any commercial or financial relationships that could be construed as a potential conflict of interest.

The authors declare that this study received funding from China Three Gorges Construction Engineering Corporation. The funder had the following involvement in the study: KL and HP are employed by China Three Gorges Construction Engineering Corporation. HP provided relevant documents of the Jinpingzi landslide. KL analyzed the test data. They were also involved in corrections, modifications, and final acceptance.